NETL

NATIONAL ENERGY TECHNOLOGY LABORATORY

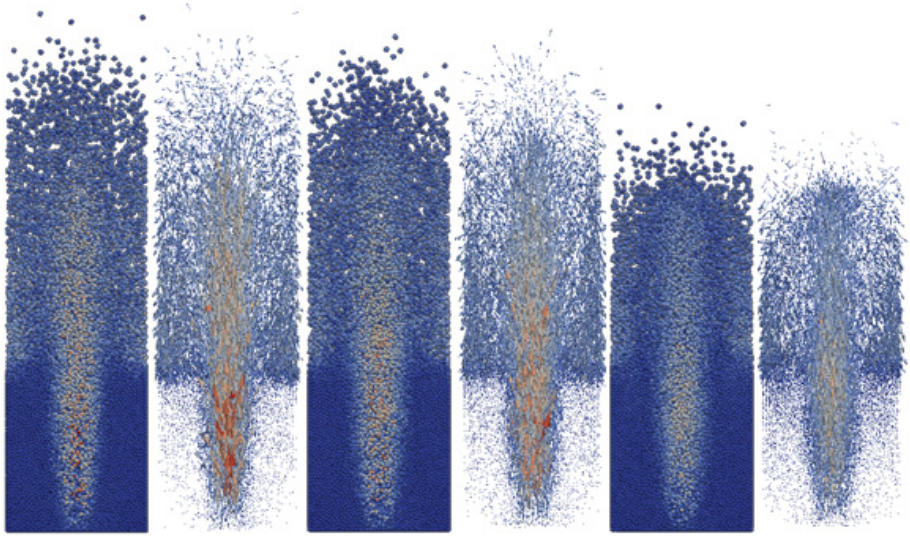

Validating the MFiX-DEM Model for Flow Regime Prediction in a 3D Spouted Bed

8 February 2018

U.S. DEPARTMENT OF ENERGY | NATIONAL ENERGY TECHNOLOGY LABORATORY

Office of Fossil Energy

NETL-PUB-21381

Disclaimer

Cover Illustration: Particle positions and velocity vectors of the different spouting regimes observed in the 3D spouted bed for different operating conditions

Suggested Citation: Banerjee, S.; Guenther, C; Rogers, W.A. *Validating the MFiX-DEM Model for Flow Regime Prediction in a 3D Spouted Bed*; NETL-PUB-21381; NETL Technical Report Series; U.S. Department of Energy, National Energy Technology Laboratory: Morgantown, WV, 2018.

Validating the MFiX-DEM Model for Flow Regime Prediction in a 3D Spouted Bed

Subhodeep Banerjee[1,2], Chris Guenther[1], William A. Rogers[1]

[1]Research and Innovation Center, National Energy Technology Laboratory

[2]Oak Ridge Institute for Science and Education

NETL-PUB-21381

8 February 2018

NETL Contacts:

Subhodeep Banerjee, Principal Investigator

William Rogers, Task Lead

Jonathan Lekse, Technical Portfolio Lead

This page intentionally left blank

Table of Contents

List of Figures

List of Tables

Acronyms, Abbreviations, and Symbols

Term	Description
CLC	Chemical looping combustion
DEM	Discrete element method
d_p	Particle diameter, m
$e_{n,p\leftrightarrow p}$	Particle-particle coefficient of restitution, dimensionless
$e_{n,p\leftrightarrow w}$	Particle-wall coefficient of restitution, dimensionless
$\mathbf{F}_C$	Net contact force, N
$\mathbf{F}_D$	Net drag force, N
$\mathbf{F}_T$	Total force, N
g, $\mathbf{g}$	Acceleration due to gravity, m/s²
k_n	Spring stiffness coefficient, N/m
L	Bed length/height, m
m	Particle mass, kg
MFiX	Multiphase Flow with Interphase eXchanges
p	Pressure, Pa
t	Time, s
u_{bg}	Background velocity, m/s
u_{mf}	Minimum fluidization velocity, m/s
u_{sp}	Spouting velocity, m/s
$\mathbf{V}$	Particle velocity, m/s
$\mathbf{X}$	Particle position, m
ε_{mf}	Solids volume fraction at minimum fluidization, dimensionless
$\mu_{p\leftrightarrow p}$	Particle-particle coefficient of dynamic friction, dimensionless
$\mu_{p\leftrightarrow w}$	Particle-wall coefficient of dynamic friction, dimensionless
ρ_f	Fluid phase density, kg/m³
ρ_p	Particle density, kg/m³

Acknowledgments

This work was completed as part of National Energy Technology Laboratory (NETL) research for the U.S. Department of Energy's (DOE) Carbon Storage Program. This project was supported in part by an appointment to the Research Participation Program at NETL administered by the Oak Ridge Institute for Science and Education (ORISE) through an inter-agency agreement between the DOE and EPA.

EXECUTIVE SUMMARY

The spout-fluidized bed reactor with relatively large oxygen carrier particles offers several advantages in chemical looping combustion operation using solid fuels. The large difference in size and weight between the oxygen carrier particles and the smaller coal or ash particles allows the oxygen carrier to be easily segregated for recirculation; the increased solids mixing due to dynamic flow pattern in the spout-fluidization regime prevents agglomeration. The primary objective in this work is to determine the effectiveness of the MFiX-DEM model in predicting the flow regime in a spouted bed. Successful validation of the code will allow the user to fine tune the operating conditions of a spouted bed to achieve the desired operating condition.

The 3D spouted bed simulation in MFiX-DEM is set up based on a previous flow regime mapping experiment using 4-mm-diameter glass beads as the bed material. The minimum fluidization velocity of the particles in the simulation is determined by monitoring the pressure drop across the bed as the fluidizing velocity is increased. At the minimum fluidization condition, the pressure drop starts to deviate from a linear relationship with velocity and flattens out as the bed transitions from the packed configuration to a fluidized one. The operating conditions in the simulation are normalized based on the minimum fluidization velocity in order to account for differences in the particle size and weight in future work.

The flow regimes predicted by the simulation show excellent agreement with the experimental flow regime map at every operating condition. Spectral analysis of the pressure fluctuations in the bed is performed to quantitatively corroborate the visual observations of the flow pattern based on the particle trajectories. The qualitative trends in the shape, frequency, and power of the dominant peak in the frequency spectra follow the expectations from theory and experiment. The results presented in this work confirm that the MFiX-DEM model can effectively predict the flow regime in a spouted bed with high accuracy.

A reduced value of the spring stiffness coefficient, required for the particle collision calculations, is used in this work as it would take months to complete the simulations with the exact value. A parametric study is conducted on the spring stiffness to rule out errors in the results due to the reduced value. It is found that the value used as a starting point in the simulation was sufficient to produce accurate results and increasing the value does not affect the results, even in the worst case scenario. All other parameters used in the simulation were based on the exact physical values.

1 INTRODUCTION

The rate of fuel conversion in the coal-direct chemical looping combustion (CLC) process is limited by the char gasification step (Leion et al., 2009). The agglomeration between oxygen carrier and coal ash is also a concern as it has been reported to reduce the reactivity of the metal oxide particles (Rubel et al., 2011). These concerns can be addressed by employing a spout-fluidized bed reactor with relatively large oxygen carrier particles, unlike in CLC using gaseous fuels that can use a bubbling bed or fast fluidized bed reactor. The relatively larger particles of the oxygen carrier have additional benefits such as easier separation of the smaller coal and ash particles from the recirculating oxygen carrier. The increased friction from the dynamic mixing of solids in a spout-fluidized bed can also serve to slough off the ash build-up on the metal oxide particles and restore reactivity (Shen et al., 2009).

Based on their diameter and density, the larger oxygen carrier particles can be classified as Group D particles according to Geldart's powder classification (Geldart, 1973). The spouted bed was originally proposed as an alternative to overcome the limitation of a typical bubbling or fast fluidized bed to handle particles larger than a few hundred micrometers in diameter (Mathur & Gishler, 1955). In spout-fluidization, a high velocity gas stream is utilized to create a localized high velocity region at the center of the bed known as the spout where the particles and voids move in a structured manner with little radial displacement (Sutkar et al., 2013).

The flow pattern in a spouted bed can be broadly classified into different flow regimes depending on the operating conditions, specifically the background velocity and the spouting velocity. The physical appearances of the main five flow regimes are presented in Figure 1 Physical appearance of the main five flow regimes

and described below. There is some discrepancy in the names associated with the different flow regimes in the literature but the physical and dynamic characteristics of the flow are similar. The nomenclature used in Link et al. (2005) is used in this report.

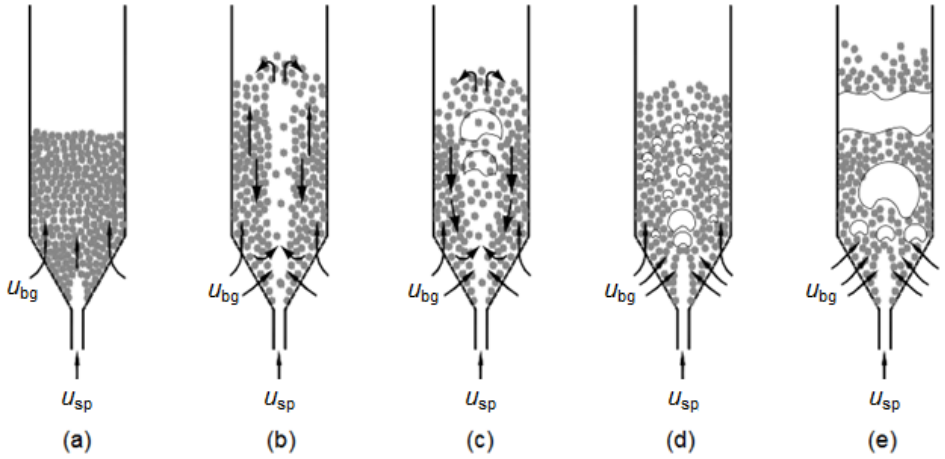

Figure 1 Physical appearance of the main five flow regimes

(a) Fixed bed/internal spout: At background fluid velocities far below the minimum fluidization velocity, the particles in the bed do not move. As the spouting velocity is increased keeping the background velocity low, an internal cavity is formed with a strong and densely packed arch that does not penetrate through the bed. This is a stable particle configuration where only the particles in the spout channel are moving.

(b) Spouting with aeration: With a sufficiently high spouting velocity and low background velocity, the spout channel penetrates the entire length of the bed. The spout and annulus form distinct zones with movement occurring only in the particles in and adjacent to the spout channel. This is a stable particle configuration and there is only a slight fluctuation in pressure drop with no periodicity.

(c) Spout-fluidization: If the spouting velocity remains high and the background velocity is also increased, the particles in the upper part of the annulus are also fluidized and move gently. The spout channel grows wider and is periodically blocked by downward flowing particles in the annulus. The pressure fluctuations are small but regular with a clear dominant frequency associated with the time taken to remove the particle blockage in the spout.

(d) Jet in fluidized bed: As the background velocity increases further, the spouting and fluidized (bubbling) behaviors overlap with all particles in motion and continuous bubble formation in the annulus. The spout channel is still present but is periodically blocked and/or diverted through the annulus. The bubbles are smaller than in the slugging regime so the frequency associated with pressure fluctuations is higher. The frequency spectrum for the jet in fluidized bed regime can be different for comparable operating conditions given the relative frequencies of bubble formation and spout blockage.

(e) Slugging bed: With a high background velocity and very low spout velocity, the spout channel collapses allowing the bubbles in the annulus to coalesce into large bubbles known as slugs equal in size to the bed diameter, which cause particles across the whole cross-section to move up and down. Since the slugs take more time to form and propagate, the large pressure fluctuations associated with the slugging bed regime have a distinct periodic behavior with a lower dominant frequency.

The objective of this study is to investigate gas-solid spouted beds using the MFiX-DEM framework and demonstrate its effectiveness in predicting the flow regimes in the bed for different values of the background velocity and the spouting velocity. The DEM version of MFiX has been previously validated for the simulation of spouted beds with wet granular-fluid flows (Zhang & Li, 2017). The pressure fluctuations in the bed are recorded for each different operating condition and converted into a frequency spectrum using a Fourier transform. The shape and frequency of the peak with the largest power are matched against the characteristics of the different flow regimes summarized in Table 1 in order used to identify the associated flow regime. The quantitative results are corroborated by visualizing the particle movement in the spouted bed apparatus.

Table 1 Identifying characteristics of the flow regimes in a spouted bed

Regime	Peak frequency	Shape	Power
Internal spout	No peak	No peak	Low
Spouting with aeration	No peak	No peak	Low
Spout-fluidization	High	Narrow (< 0.5 Hz)	High
Slugging bed	Low	Broad (> 1 Hz)	High
Jet in fluidized bed	Intermediate	Intermediate	High

2 COMPUTATIONAL SETUP

The flow regime predictions from the MFiX-DEM simulations are validated against the experimental study of Link et al. (2005). The 3D experimental apparatus consists of a fluidized bed as shown in Figure 2. A uniform grid is established consisting of 14 elements in the x-direction, 100 elements in the y-direction and 7 elements in the z-direction. Such a coarse grid is required to resolve the motion of the relatively large particles in the system in the DEM framework. The complete properties of the glass particles used in the experiment and their corresponding simulation values are given in Table 2. The initial particle configuration is generated by releasing a block of 42,840 4-mm-diameter particles and running the simulation without any fluidizing air for 0.5s to allow the particles to settle into a randomly distributed packed bed; the height of the initial packed bed configuration is around 18.2 cm with a solids volume fraction ε_s of around 0.61.

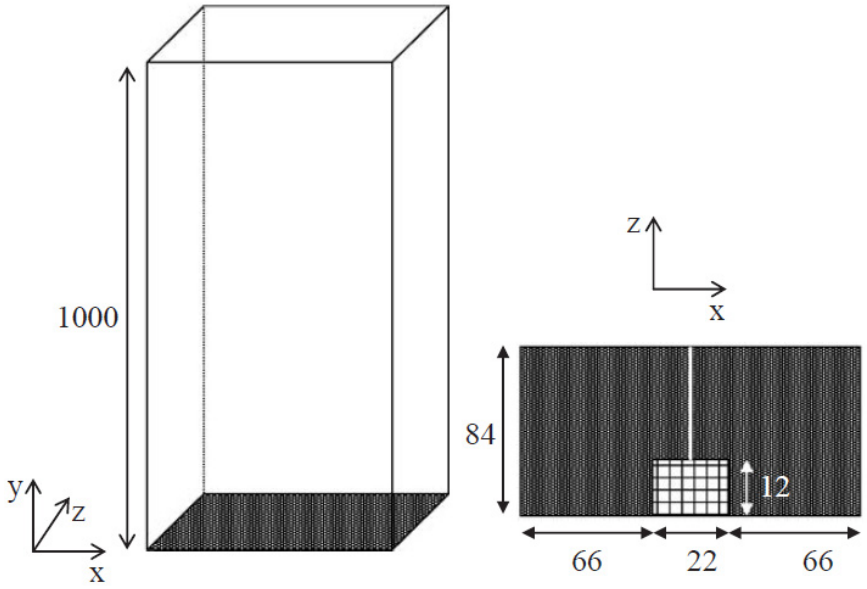

Figure 2 Experimental geometry of the 3D spout-fluidized bed (dimensions are in mm)

Table 2 Properties of the glass particles used in the experiment and simulation

Property	Experiment	Simulation
d_p (mm)	4.04 ± 0.02	4.0
ρ_p (kg/m³)	2526 ± 1	2500
u_{mf} (m/s)	1.77 ± 0.03	1.97
$e_{n,p\leftrightarrow p}$	0.97 ± 0.01	0.97
$e_{n,p\leftrightarrow w}$	0.97 ± 0.01	0.97
$\mu_{p\leftrightarrow p}$	0.10 ± 0.01	0.10
$\mu_{p\leftrightarrow w}$	0.10 ± 0.01	0.10
# particles	44,800	42,840

The bed is fluidized with air through three regions. A homogeneous gas distribution over the two shaded regions in the cross-section in Figure 2 provides the background velocity. The spouting velocity is supplied over the 22 × 12 mm region located on the front wall on the border between the two fluidization sections. In the experiment, a pressure probe is located in the center of the back wall about 10 mm above the base plate; the pressure readings in the simulation are taken from the middle of the bottom-most, back-most element at $(x, y, z) = (0{,}5{,}78)$ mm.

In MFiX-DEM, the Navier-Stokes equations for conservation of mass and momentum of the gas phase are slightly modified to account for the presence of the particles by including the volume fraction of the gas phase, and additional source terms are included in the momentum equation to account for drag from the solid phase (Garg et al., 2012). The energy equation is not required for this work. The solid phase comprises the individual particles represented in a Lagrangian frame of reference, their position and velocity evolving with time based on force balance calculations.

$$\frac{d}{dt}\big(\mathbf{X}(t)\big) = \mathbf{V}(t) \tag{1}$$

$$m\frac{d}{dt}\big(\mathbf{V}(t)\big) = \mathbf{F}_{\mathrm{T}} = m\mathbf{g} + \mathbf{F}_{\mathrm{D}}(t) + \mathbf{F}_{\mathrm{C}}(t) \tag{2}$$

where $\mathbf{F}_{\mathrm{D}}$ is the total drag force due to pressure and viscous effects on the particle and $\mathbf{F}_{\mathrm{C}}$ is the net contact force from collisions with other particles or the wall. The contact forces on each particle is calculated explicitly in the DEM framework, which differentiates it from other Lagrangian simulation. The soft-sphere collision model is used to resolve the contact forces in this work; it is preferred over the hard-sphere model as it is better suited for non-dilute systems. The details of its implementation are available in the MFiX-DEM documentation (Garg et al., 2012).

The interphase transfer of momentum is governed by the interphase exchange coefficient, which can be modeled by one of various empirical relations. The Gidaspow model (1992) is used in this study as it is ideal for fluidized bed simulations that include a range of solid loadings because it accounts for the differences in the solid-gas interaction behavior in the dilute and densely packed regions by switching between the drag prediction of the Ergun equation (1952) and the drag model of Wen and Yu (1966) based on the solids volume fraction. To ensure increased accuracy in the solid-gas coupling, instead of using the local cell-averaged gas-phase velocity in calculating the viscous force on each particle, the gas phase velocity is first interpolated to the particle location. The pressure drag is evaluated at the cell-center. The net total drag force on all particles in a cell is incorporated in the gas phase momentum equation as the source term (Garg et al., 2012).

3 RESULTS & DISCUSSION

3.1 Minimum fluidization velocity

Once the particles are stabilized in a randomly distributed packed bed configuration, the minimum superficial velocity required to fluidize the particles can be calculated. As gas is injected into the bed, the pressure drop across the bed increases with the gas velocity until the minimum fluidization condition is reached and the net weight of the bed is exactly balanced by the pressure drop. Increasing the fluidizing velocity further does not produce any further increase in the pressure drop; there might even be a slight decrease as the particles begin to separate and fluidize. Bubbles can start to form at higher fluid velocities and cause the pressure drop to fluctuate but the average value should remain constant.

The minimum fluidization velocity obtained experimentally is 1.77 m/s (Link et al., 2005). In the MFiX-DEM simulation, the minimum fluidization condition is determined by fluidizing the bed at increasing velocity increments across the inlet in both spout and background velocity regions until the pressure at the base of the bed stops increasing with increased fluidizing velocity and starts to stagnate. The variation in the bed pressure with velocity is shown in Figure 3. Based on the point where the pressure starts to deviate from the red line of best fit, the minimum fluidization velocity for the particles used in the simulation is 1.95 m/s. A possible source of error for the slight discrepancy of around 10% in this value could be the empirical drag law as it affects the momentum imparted to the particles by the gas phase.

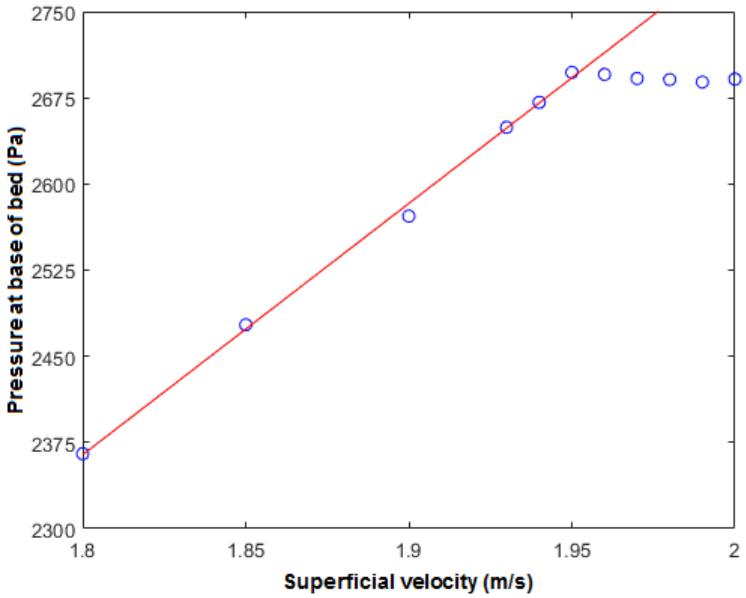

Figure 3 Obtaining minimum fluidization velocity from pressure drop measurements

At the minimum fluidization condition, the pressure drop is exactly balanced by the weight of the bed by definition. Hence,

$$\frac{\Delta p}{L} = \left(1 - \varepsilon_{mf}\right)\left(\rho_p - \rho_f\right)\mathrm{g}$$

The height of the bed expands slightly to around 18.4 cm at minimum fluidization; the corresponding pressure drop Δp is 2.70 kPa. Substituting for the physical densities of the particles and fluid (air), the solids volume fraction at minimum fluidization ε_{mf} is 0.60.

The quantitative measure of the minimum fluidization velocity is corroborated by visualizing the particle movement in the bed as shown in Figure 4. At fluid velocities up until just below the minimum fluidization velocity, particle movement is aberrant and limited only to a few particles. Once the minimum fluidization condition reached, the particles exhibit fluid-like motion inside the bed with increasing particle velocities as the fluid velocity also increases.

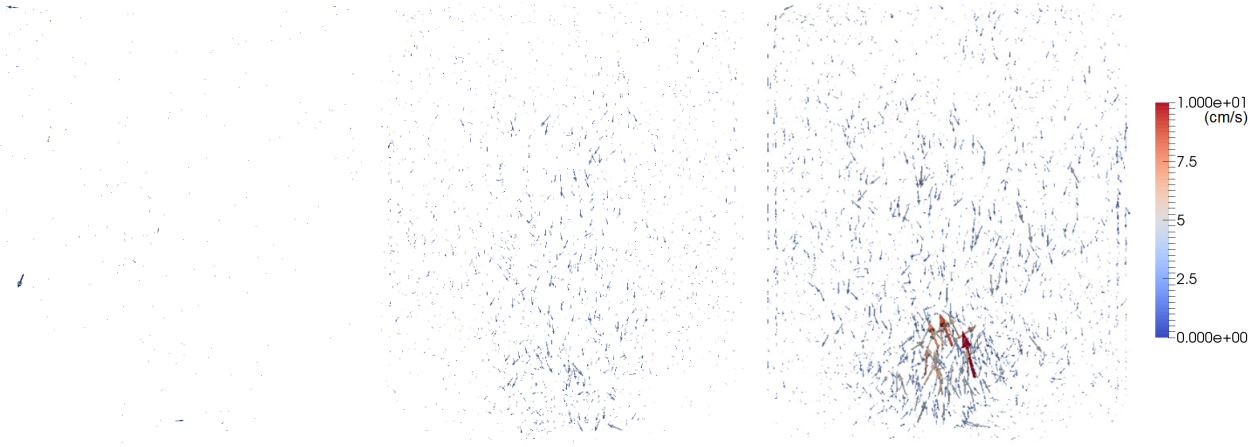

u = 1.95 m/s u = 1.96 m/s u = 1.97 m/s

Figure 4 Onset of particle movement at minimum fluidization condition

3.2 Flow regime prediction

The fluidization in the spout-fluidized apparatus shown in Figure 2 was assessed experimentally over a wide range of operating conditions with and without a spout (Link et al., 2005). The complete regime map resulting from spectral analysis of the experimental data is given in Figure 5. At most operating conditions, one of the flow regimes described in section 1 can be clearly identified; the rest was categorized as an intermediate regime between the stable spouting with aeration regime with weak periodicity in the pressure drop fluctuations and the spout-fluidization regime with a clear dominant frequency. The flow regime map is used to select operating conditions for the simulations to assess the capability of MFiX-DEM to reproduce the experimentally observed flow regimes. Six test cases are chosen to cover each of the five flow regimes associated with a spouted bed shown in Figure 1 Physical appearance of the main five flow regimes

and the intermediate regime between the steady spouting with aeration regime and the dynamic spout-fluidization regime; they are marked on Figure 5 and listed in Table 3.

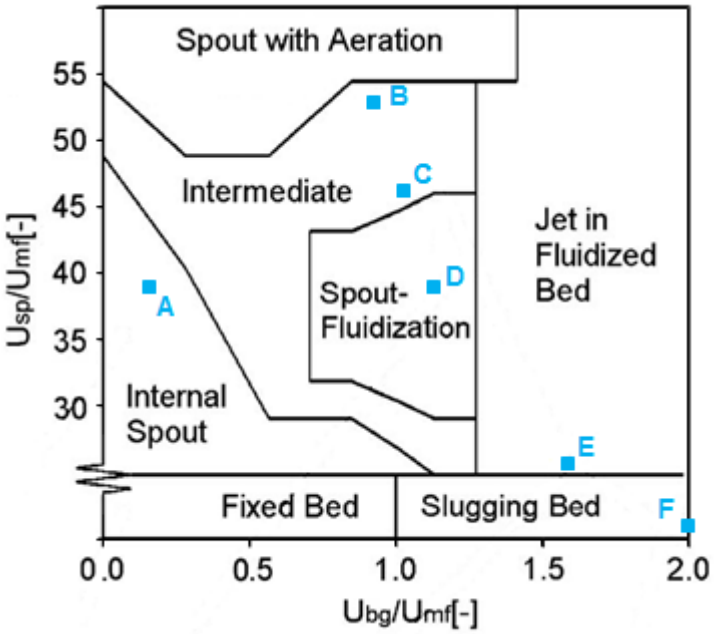

Figure 5 Experimental regime map of the 3D bed (Link et al., 2005) with simulation cases labeled

Table 3 Test cases for MFiX-DEM simulation

Case	u_{bg} (m/s)	u_{bg}/u_{mf}	u_{sp} (m/s)	u_{sp}/u_{mf}
A	0.3	0.15	76	39
B	1.8	0.9	103	53
C	2.0	1.0	90	46
D	2.2	1.1	76	39
E	3.1	1.6	41	34
F	3.9	2.0	3.9	2.0

3.2.1 Case A: internal spout

Figure 6 shows the location and the velocity vectors of the particles inside the 3D bed for case A. The spout channel is clearly evident but it does not penetrate through the bed. Instead, the kinetic energy of the particles goes towards loosening the closely packing resulting in the bulging at the center compared to the original packed configuration. Since the background velocity is significantly lower than the minimum fluidization velocity, there is no particle movement in the annulus, which remains tightly packed. The pressure drop spectrum at the base of the bed is shown in Figure 7. The internal spout regime is a stable regime with little to no pressure fluctuations.

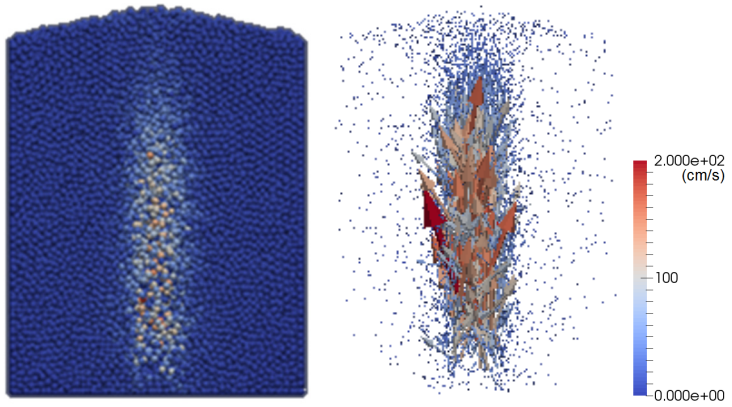

Figure 6 The particle positions and velocity vectors of case A show an internal spout

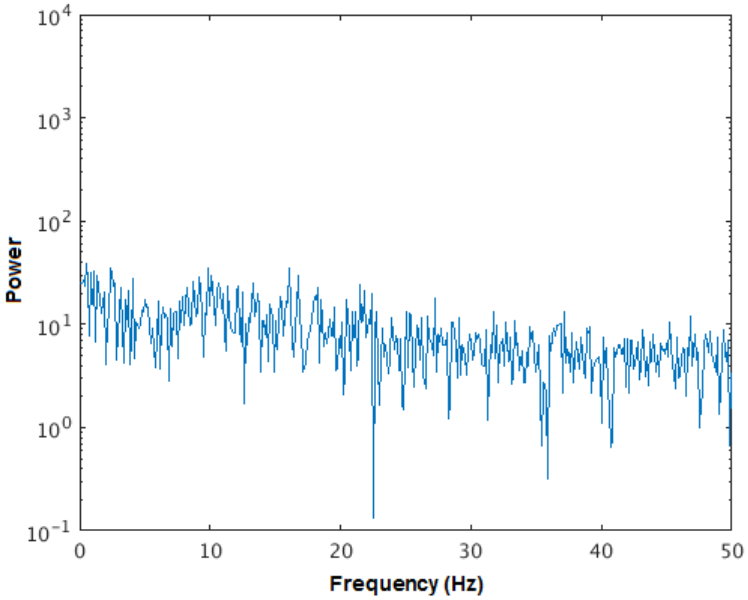

Figure 7 The frequency spectrum of the pressure drop fluctuations of case A shows no periodicity

3.2.2 Case B: spouting with aeration

Snapshots of the particle positions and velocity vectors for cases B, C, and D are given in Figure 8. In all these cases, the spout channel penetrates the entire bed and forms a fountain above the bed that deposits the particles back into the annulus. The particle trajectories in these cases are nearly identical since they all represent spouted bed configurations; additional information is required to categorize the flow regimes for each different operating condition such as the pressure spectra or vertical particle flux in the annulus. It can be seen from Figure 8a that case B has the highest particle velocity in the spout and the least particle movement in the annulus. A very fast spout with no fluidization in the annulus is characteristic of the spouting with aeration regime. The frequency spectrum of the pressure drop fluctuations of case B is given in Figure 9. It shows a somewhat broad peak with a power of around 200 at a high frequency. Although the peak indicates slight periodicity, the very low power indicates a very stable spout, which puts this configuration in the spouting with aeration regime.

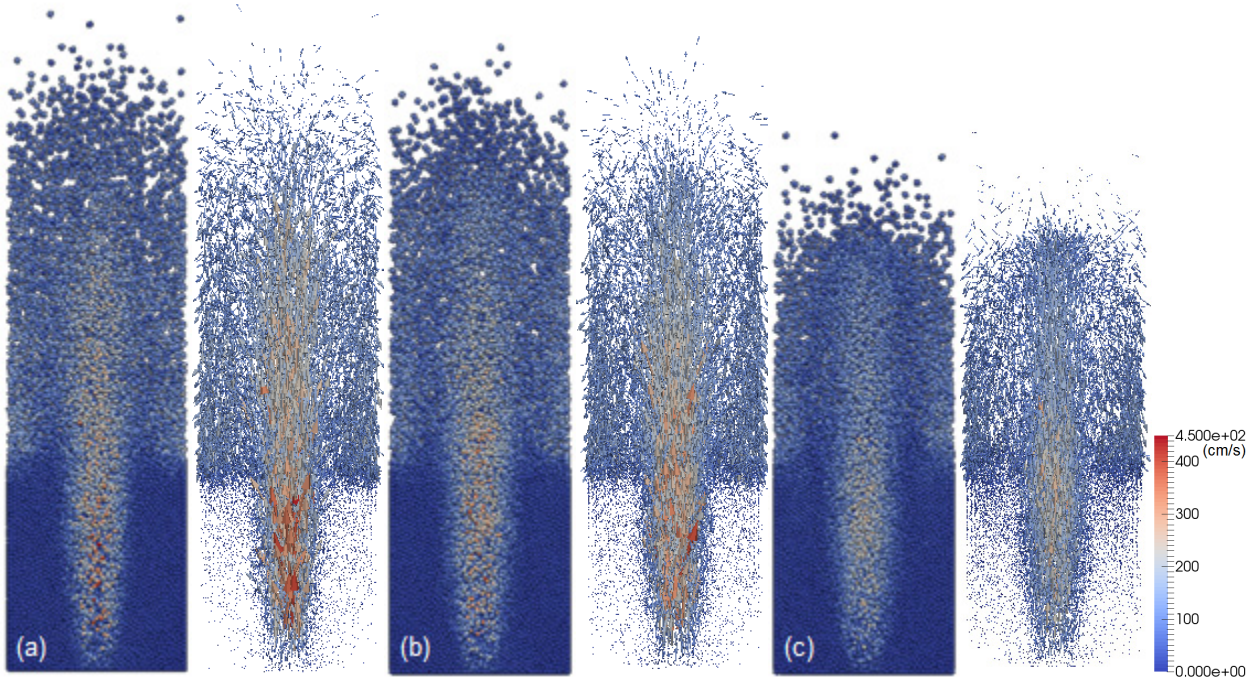

Figure 8 The particle positions and velocity vectors of cases B (a), C (b), and D (c) show spouting behavior

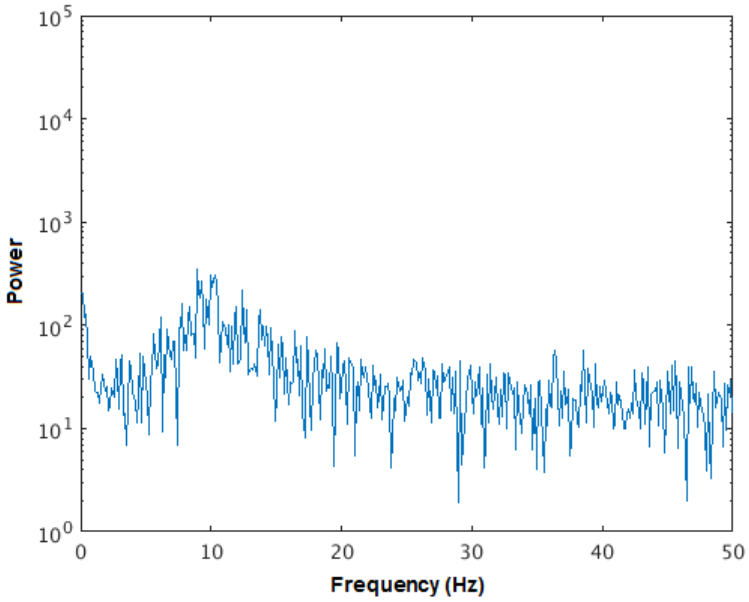

Figure 9 The frequency spectrum of case C shows a peak at high frequency with very low power

3.2.3 Case C: intermediate spouting

Figure 8b shows a weaker spout compared to the spouting with aeration regime and increased particle movement in the annulus. The spout is wider due to more particles from the annulus being entrained by the spout. The increased annular velocity also results in slight necking at the base of

the spout where particles from the annulus periodically block the spout. The frequency spectrum of the pressure drop fluctuations at the back of the bed is given in Figure 10. The peak in Figure 10 is more distinct compared to the spouting with aeration regime: it is narrower with a power of around 900. The increased periodicity is associated with the intermittent blockage of the spout by the entrained particles but it does not show a clear dominant frequency as is expected for spout-fluidization. It can be concluded that case C falls in the intermediate regime between spouting with the aeration and spout-fluidization regimes.

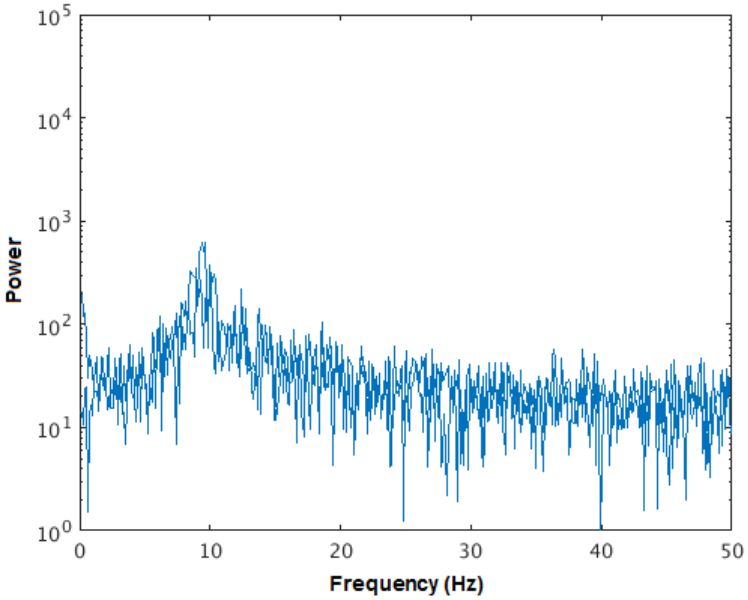

Figure 10 The frequency spectrum of case C shows a peak at high frequency with low power

3.2.4 Case D: spout-fluidization

It can be seen from Figure 8c that the particle movement in the annulus is significantly improved in case D with only particles near the bottom corners of the bed not exhibiting motion. On the other hand, the particle velocity spout is lower and the fountain reaches a lower height. The combination of a lower spout velocity and increased fluidization in the annulus allows more particles from the annulus to be entrained by the spout. The neck formation periodically blocking the spout is clearly visible in Figure 8c as the particles entering from the annulus at the base of the spout have almost zero velocity. The frequency spectrum of the pressure drop fluctuations given in Figure 11 shows a clear dominant frequency at 6.5 Hz with a large power of around 4000 associated with the little time taken to remove the periodic blockage from the spout. A second harmonic peak is also visible. The presence of a narrow dominant peak in the pressure spectrum incontrovertibly puts case D in the spout-fluidization regime. The frequency of the dominant peak shows excellent agreement with the experimental data, which shows a similar narrow peak at 5–6 Hz (Link et al., 2005). Quantitative agreement in the power is not possible since the power of the spectrum is dependent on the number of data points used in the Fourier transform. However, the relative power of the frequency spectra for cases B through D are in accordance with the expected results.

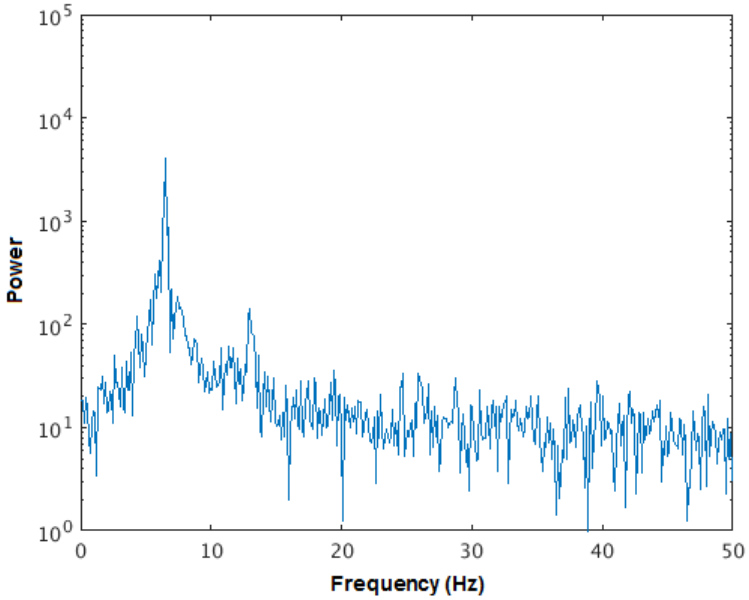

Figure 11 The frequency spectrum of case D shows a narrow peak at high frequency with high power

The lower particle velocity in the spout and the increased fluidization in the annulus are both essential to achieve spout-fluidization. The narrow range of operating conditions at which the spout-fluidization regime can be sustained is seen on the experimental flow regime map given in Figure 5 and confirmed by simulation by increasing the spouting velocity from 76 m/s used in case D to 86 m/s while keeping the same background velocity. On the corresponding pressure frequency spectrum shown in Figure 12, the peak is slightly broader and shifted to 8.0 Hz with a lower power of around 1600, which indicates that there is no clear dominant frequency and the spout blockage is removed faster by the fast moving particles. This behavior is closer to the intermediate regime than that of spout-fluidization.

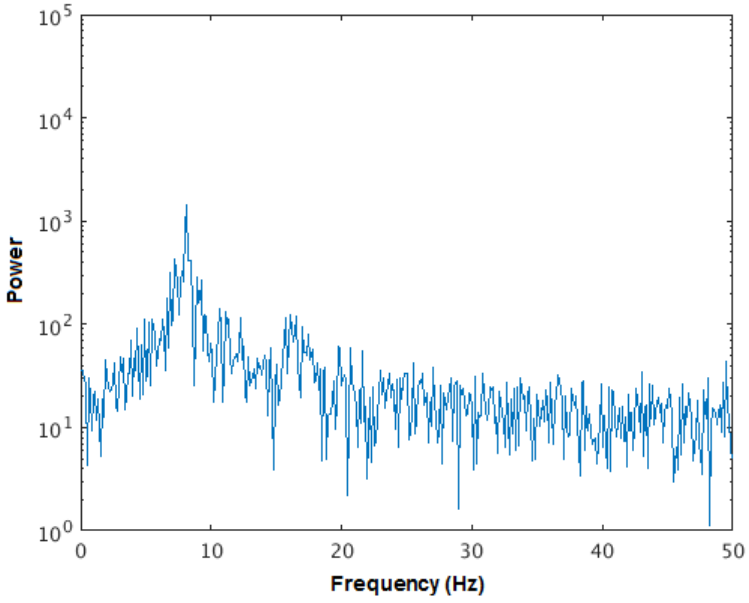

Figure 12 Increasing the spouting velocity causes the flow to revert to the intermediate regime

3.2.5 Case E: jet in fluidized bed

Figure 13 shows the particle velocity vectors in case E. The particle trajectories shown at 2s time intervals reveal a rapidly changing flow pattern. The annulus is fully fluidized and all particles are moving. The void spaces seen in Figure 13 are due to the formation of bubbles in the annulus. At the same time, a spout channel is present but it is periodically diverted through the annulus. The flow pattern is thus an overlap of a spouted bed and a fluidized (bubbling) bed and can be characterized as the jet in fluidized bed regime.

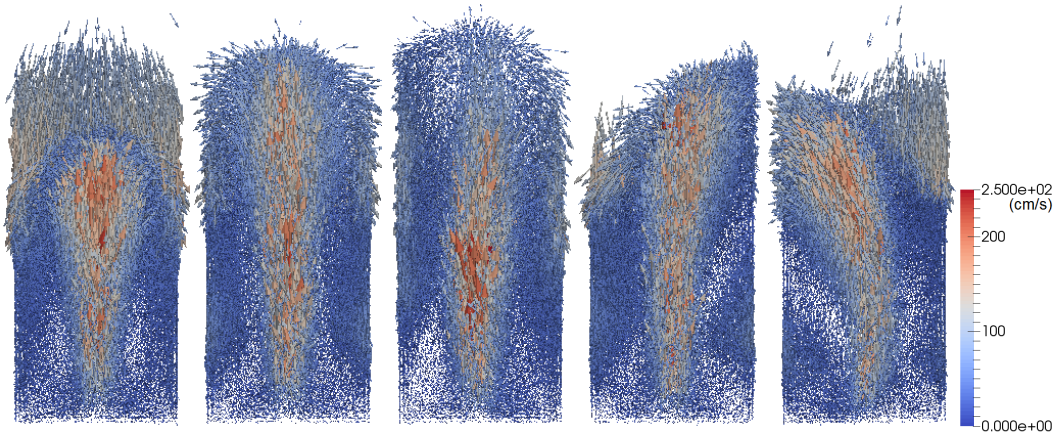

Figure 13 The particle velocity vectors of case E show rapidly changing spout shapes (t = 2s, 4s, 6s, 8s, 10s)

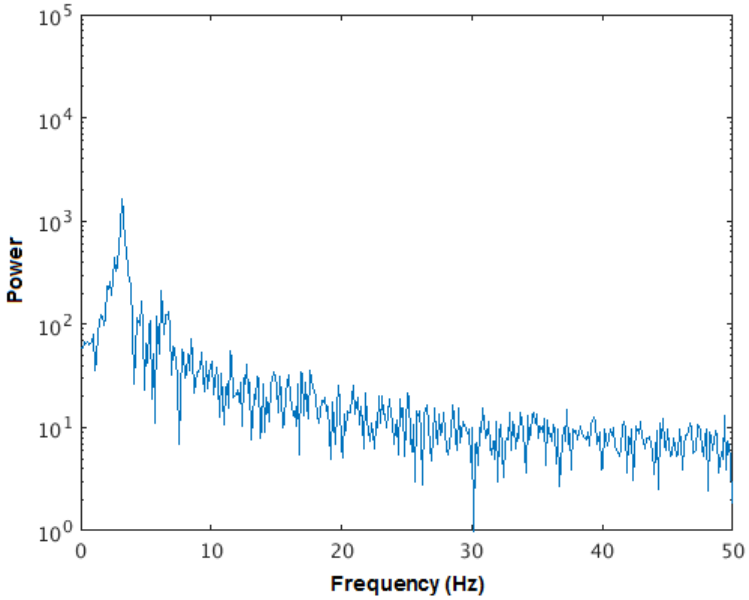

Figure 14 The frequency spectrum of case E shows a wide peak at medium frequency with high power

Periodicity in the pressure drop in the jet in fluidized bed regime is associated with both bubble formation and spout blockage. Depending on the relative strength of these periodic influences on the pressure drop, the jet in fluidized bed regime can exhibit a single, double, or even multiple peaks for comparable operating conditions. The pressure frequency spectrum of case E in Figure 14 shows

a slightly wide peak at 3.1 Hz with a high power of around 1600. The dominant frequency is lower than the spout-fluidization case and is likely due to bubble formation since the bubbles take some time to form and propagate. There is a second smaller peak around 8 Hz, which could be the frequency associated with spout blockage by particle entrainment.

3.2.6 Case F: slugging bed

The uniform fluidizing velocity of twice the minimum fluidization velocity across the inlet in case F causes the particles to shoot up rapidly across the width of the bed forming large bubbles known as slugs. Hence, case F indicates a slugging bed regime. The formation of a slug is shown in Figure 15. A bubble of gas starts to form in the bed and lift the particles upwards at about t = 2.1s following the collapse of the previous slug. The bubble grows as it travels upwards and by 2.2s, the slug has expanded to more than the width of the bed. Once the slug has reached the top of the bed around 2.3s, it bursts allowing the particles to drop rapidly back into the bed before the next bubble starts to take shape around 2.5s.

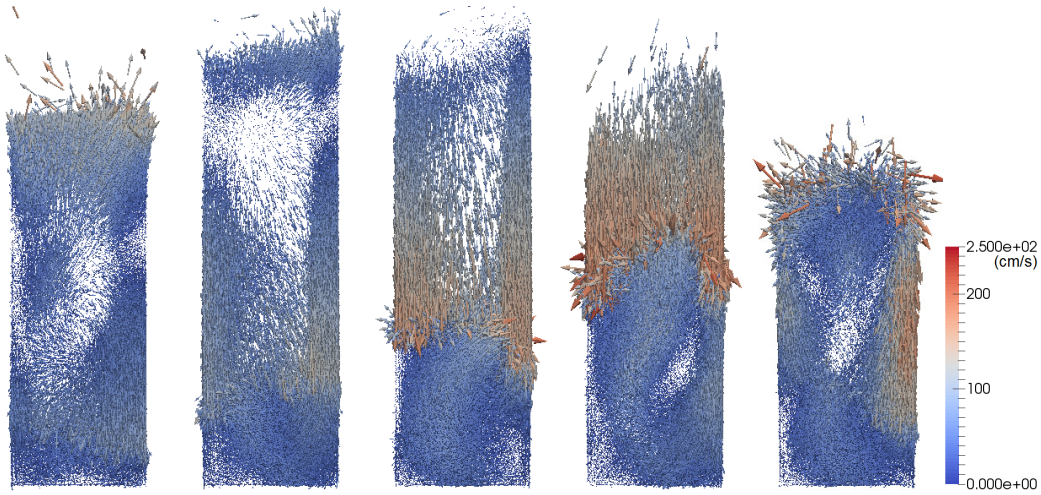

Figure 15 The velocity vectors for case F showing the formation of a slug (t = 2.1s, 2.2s, 2.3s, 2.4s, 2.5s)

The pressure drop fluctuations of case F are represented in the frequency spectrum in Figure 16. There is a wide peak (actually twin peaks) around 1.6–3.0 Hz with a high power of around 5,000. The low frequency is characteristic of the slugging bed regime since the large slugs take time to form and travel the length of the bed and agrees well quantitatively with the experimental value of 1.5 Hz (Link et al., 2005). Furthermore, the qualitative trends in frequency and power between the spout-fluidization regime, the jet in fluidized bed regime, and the slugging bed regime line up with the identifying characteristics listed in Table 1.

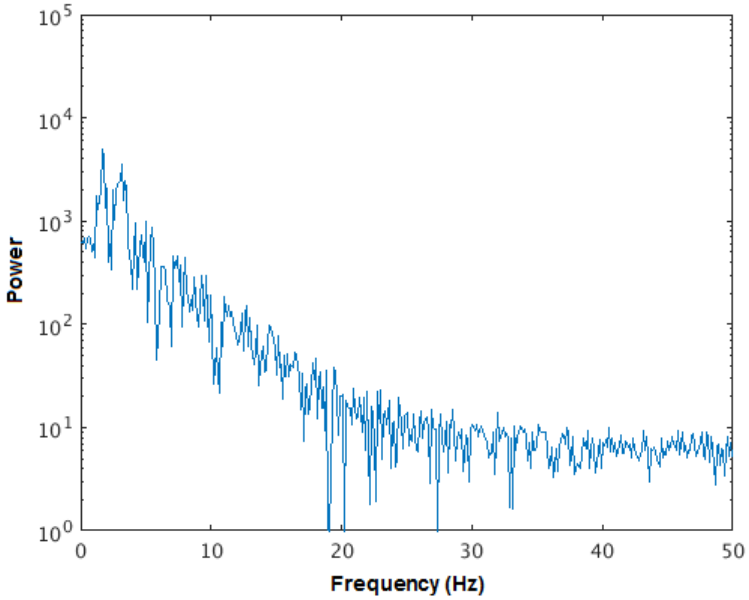

Figure 16 The frequency spectrum of case F shows wide (twin) peaks at low frequency with high power

3.3 Influence of the particle spring stiffness coefficient

In the soft-sphere collision approach, the overlap between the colliding particles is represented as a spring-dashpot system in both normal and tangential directions. The spring causes the rebound of the colliding particles and the dashpot mimics the dissipation of kinetic energy due to inelastic collisions (Garg et al., 2012). However, using a spring stiffness coefficient for the particles close to the real physical values derived from the Young's modulus in the simulation would require a very small particle time step, which would require several months for a system with thousands of particles. A spring stiffness value of k_n = 10,000 N/m, twice the value required for the solution to be stiffness-invariant in Bokkers (2005), was used as the starting point in this study and the results presented thus far. A parametric study is conducted on the spring stiffness to determine if the spring stiffness can be reduced in future simulations to take advantage of the significant reductions in wall time that would be afforded. Other particle collision parameters such as the coefficients of restitution and friction are based on real values *and* do not affect the wall time so they are not considered for parametric study.

3.3.1 Influence on the minimum fluidization velocity

The steps to determine the minimum fluidization velocity outlined in section 3.1 are repeated with a spring stiffness value of k_n = 100 N/m, two orders of magnitude lower than the starting value. Figure 17 shows the change in bed pressure with increasing superficial velocity in these simulations. It is noted that these simulations were erroneously run with a slightly smaller cross-sectional area based on the pseudo-2D setup of Link et al. (2005) than the actual 3D geometry shown in Figure 2. As a result, the absolute values of the pressure are higher compared to Figure 3 but the behavior that is used to ascertain the minimum fluidization condition is unaffected. From Figure 17, the pressure increases linearly with the superficial velocity until approximately 1.97 m/s at which point the minimum fluidization condition is achieved and the pressure flattens out/dips slightly. Hence, a decrease by two orders of magnitude in the spring stiffness only causes a 1% difference in the minimum fluidization velocity.

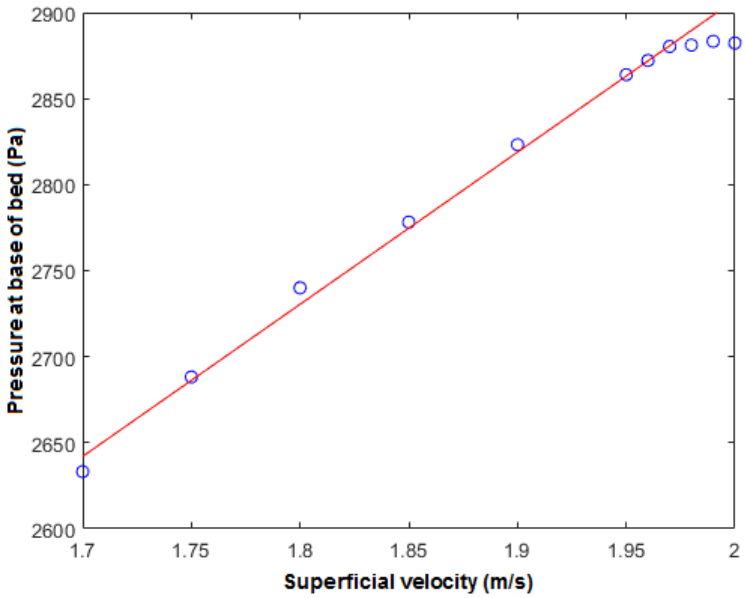

Figure 17 The minimum fluidization velocity is unaffected by a decrease in the particle spring constant

It is not surprising that the minimum fluidization velocity is unaffected by the spring stiffness based on the physics of the system. Prior to the minimum fluidization condition, the bed is loosely packed with little to no particle motion. Although particle collisions are still taking place, their relative velocities are low enough that the deformation is minimal and the contact force, regardless of the spring constant value, is negligible compared to the other forces acting on the particle such as gravity and drag (see equation (2)). A better measure of the influence of the spring stiffness can be determined by considering the spouting with aeration regime since it has the largest differences in particle speeds between the spout and annulus regions.

3.3.2 Influence on flow regime prediction

Since the largest differences in particle velocities occur in the spouting with aeration regime, a simulation is run with the same operating velocities as case B with the reduced spring stiffness value of k_n = 100 N/m. The pressure frequency spectrum given in Figure 18 shows a narrow peak at 5.0 Hz with a high power of around 5300. Additional harmonic frequencies are also visible at 10.0 and 15.0 Hz. The presence of a clear dominant peak with high power is characteristic of periodic spout blockage by particles from the annulus, which contradicts spouting with aeration behavior and instead indicates spout-fluidization.

It was seen in section 0 that a slightly weaker spout is necessary to achieve spout-fluidization. When the fast-moving particles in the spout collide with particles entrained from the annulus, the large contact force caused by the difference in speeds are more likely to repel the particles from the annulus and prevent them from causing the blockages that lead to periodic fluctuations in pressure. If the particles in the annulus are poorly fluidized on top of that as in the spouting with aeration regime, the effect is more pronounced causing very stable spouting with little periodicity. However, reducing the value of the spring stiffness diminishes the contribution of the contact force to the net force balance in the particles and allows particles from the annulus to be entrained by the spout even at high spout velocities. This explains why the simulation with the spring stiffness value of k_n = 100 N/m is unable to accurately predict the experimental flow regime.

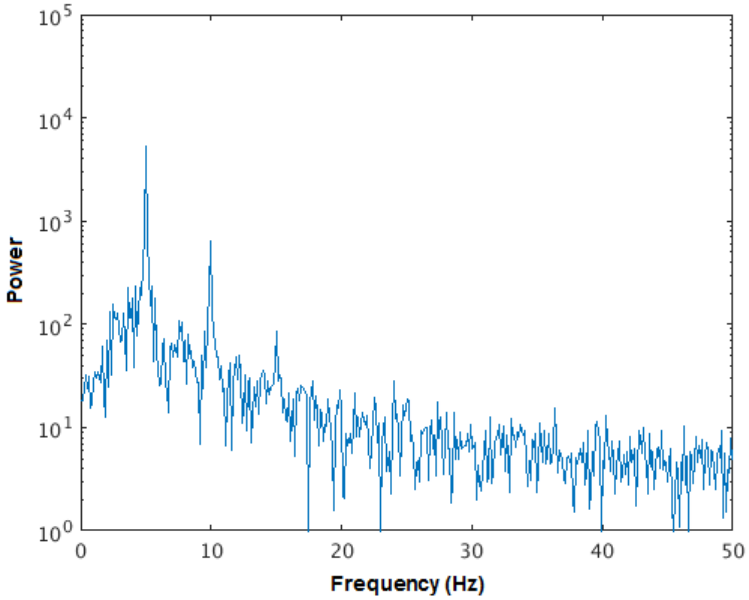

Figure 18 The reduced spring stiffness changes the flow regime from spouting with aeration to spout-fluidization

On the other hand, an increased spring stiffness value of k_n = 100,000 N/m does not significantly affect the pressure fluctuations in the bed and in turn the flow regime prediction. The pressure frequency spectrum given in Figure 19 shows a broad peak at relatively high frequency with a low power of around 200, similar to the results of case B. It can be concluded that the simulation results are relatively insensitive to values of k_n greater than 10,000 N/m. The increase in accuracy associated with increasing the spring stiffness coefficient further is marginal and does not warrant the significantly increased wall time required to complete the simulation.

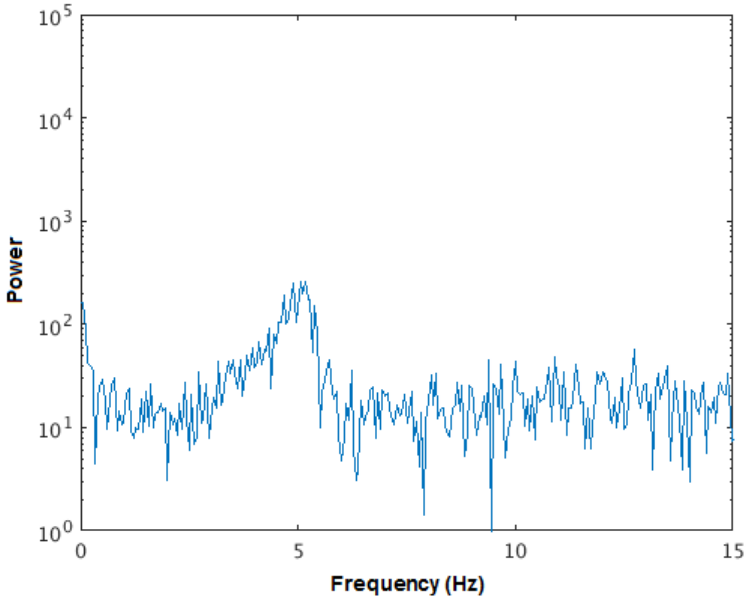

Figure 19 Increasing the spring stiffness has no significant effect on the pressure frequency spectrum

4 CONCLUSIONS

This work employs MFiX-DEM to model a 3D spouted bed to determine its effectiveness at predicting the flow regimes in the bed for a range of operating conditions. Visualizing the flow alone is not enough to identify the flow regime accurately, particularly to differentiate between the stable and unstable (dynamic) spouting behavior. Hence, spectral analysis of the pressure fluctuations in the bed is used to identify the flow regimes accurately at different operating conditions.

The operating conditions for the different flow regimes are selected based on a flow regime map determined experimentally for a laboratory-scale 3D spouted bed with glass particles by Link et al. (2005). To account for differences in the minimum fluidization velocity between the simulation and experiment, the operating conditions for each test case are normalized by the minimum fluidization velocity.

The flow regimes predicted by the MFiX-DEM model at each operating condition show excellent agreement with the experimental flow regime map. The frequency of the dominant peak in the spectral analysis also match the experimental results reasonably well in the case of the spout-fluidization, jet in fluidized bed, and slugging bed regimes although the power values cannot be directly compared as it depends on the number of data points used in the Fourier transform. Furthermore, the qualitative trends in the shape, frequency, and power of the dominant peak in the pressure frequency spectra align with the expected results in all cases. It is clear that MFiX-DEM is an effective model for predicting the flow regimes in a spouted bed with high accuracy.

5 REFERENCES

Bokkers, G. A. *Multi-level modelling of the hydrodynamics in gas phase polymerisation reactors;* Ph.D. dissertation, University of Twente: Enschede, The Netherlands, 2005.

Ergun, S. Fluid flow through packed columns. *Chem. Eng. Prog.* **1952,** *48*, 89-94.

Garg, R.; Galvin, J.; Li, T.; Pannala, S. Documentation of open-source MFIX–DEM software for gas-solids flow, 2012. https://mfix.netl.doe.gov/documentation/dem_doc_2012-1.pdf (accessed July 31, 2017).

Geldart, D. Types of gas fluidization. *Powder Technol.* **1973,** *7* (5), 285-292.

Gidaspow, D. *Multiphase Flow and Fluidization*; Academic Press: San Diego, CA, 1992.

Leion, H.; Lyngfelt, A.; Mattisson, T. Solid fuels in chemical-looping combustion using a NiO-based oxygen carrier. *Chem. Eng. Res. Des.* **2009,** *87* (11), 1543-1550.

Link, J. M.; Cuypers, L. A.; Deen, N. G.; Kuipers, J. A. M. Flow regimes in a spout–fluid bed: A combined experimental and simulation study. *Chem. Eng. Sci.* **2005,** *60*, 3425-3442.

Mathur, K. B.; Gishler, P. E. A technique for contacting gases with coarse solid particles. *AIChE J.* **1955,** *1*, 157-164.

Rubel, A.; Zhang, Y.; Liu, K.; Neathery, J. Effect of ash on oxygen carriers for the application of chemical looping combustion to a high carbon char. *Oil Gas Sci. Technol. – Rev. IFP Energies Nouv.* **2011,** *66* (2), 291-300.

Shen, L.; Wu, J.; Gao, Z.; Xiao, J. Reactivity deterioration of NiO/Al2O3 oxygen carrier for chemical looping combustion of coal in a 10kWth reactor. *Combust. Flame* **2009,** *156* (7), 1377-1385.

Sutkar, V. S.; Deen, N. G.; Kuipers, J. A. M. Spout fluidized beds: Recent advances in experimental and numerical studies. *Chem. Eng. Sci.* **2013,** *86*, 124-136.

Wen, C. Y.; Yu, H. Y. Mechanics of fluidization. *Chem. Eng. Prog. Symp. Ser.* **1966,** *62*, 100-111.

Zhang, H.; Li, S. DEM simulation of wet granular-fluid flows in spouted beds: Numerical studies and experimental verifications. *Powder Tech.* **2017**, *318*, 337-49.